

## Study of Excess Silicon at Si<sub>3</sub>N<sub>4</sub>/Thermal SiO<sub>2</sub> Interface Using EELS and Ellipsometric Measurements

V. A. Gritsenko,<sup>a,b</sup> S. N. Svitashva,<sup>b</sup> I. P. Petrenko,<sup>b</sup> Hei Wong,<sup>c</sup> J. B. Xu,<sup>d</sup> and I. H. Wilson<sup>d</sup>

<sup>a</sup>Institute of Semiconductor Physics, Novosibirsk 630090, Russia

<sup>b</sup>Department of Electronic Engineering, City University, Kowloon, Hong Kong

<sup>c</sup>Department of Electronic Engineering, The Chinese University of Hong Kong, Shatin, N.T. Hong Kong

The chemical composition and structure of the Si<sub>3</sub>N<sub>4</sub>/thermal SiO<sub>2</sub> interface in silicon/oxide/nitride/oxide (SONO) structures were studied by using electron energy loss spectroscopy (EELS) and ellipsometric measurements. Both experiments show the existence of excess silicon at the Si<sub>3</sub>N<sub>4</sub>/thermal SiO<sub>2</sub> interface, in the form of Si-Si bonds in the Si-rich silicon oxynitride. Wet oxidation of the as-deposited Si<sub>3</sub>N<sub>4</sub> has profound effects on the interfaces in SONO structure. Mechanisms responsible for these observations are proposed based on the chemical reactions during the synthesis of the SONO structure. Particularly, we propose that the Si-Si bonds are produced by replacing nitrogen with oxygen during the oxidation of Si<sub>3</sub>N<sub>4</sub>. These bonds should be the responsible candidates for the positive charge accumulation in re-oxidized nitrided oxide at the hot hole injection and ionizing radiation.  
© 1999 The Electrochemical Society. S0013-4651(98)06-067-4. All rights reserved.

Manuscript received June 17, 1998.

The oxide-nitride-oxide (ONO) structure has been widely used in the dynamic random access memory (DRAM) and electrical erasable programmable read only memory (EEPROM) devices. The ONO structures are used in DRAM as the dielectric in the three-dimensional stacked and trench memory capacitors instead of thermal SiO<sub>2</sub> and as the interpoly dielectric for multilevel metallization in complementary metal oxide semiconductors (CMOS) technology.<sup>1,2</sup> In floating gate EEPROM, the ONO structure is used as the dielectric between the floating gate and the control gate. This layer reduces the electronic discharge from the floating gate. The low leakage current of ONO structure (compared to SiO<sub>2</sub>) can be attributed to electron capturing of the traps in Si<sub>3</sub>N<sub>4</sub> and reduction of barrier transparency at the negatively biased electrode interface. Electron and hole localization on deep traps in the ONO structure can be used to write or erase the information in EEPROMs. Abnormally large trapping of electrons at the Si<sub>3</sub>N<sub>4</sub>/thermal SiO<sub>2</sub> interface<sup>3-5</sup> and hot electron and hole capturing in the ONO structure<sup>6</sup> are often reported experimentally. The nature of this phenomenon is still unclear. It is suggested that silicon oxynitride (SiO<sub>x</sub>N<sub>y</sub>) probably will be used as the gate dielectric in future memory devices for blocking boron penetration and reducing hole traps at the Si/SiO<sub>2</sub> interface. The traps in SiO<sub>x</sub>N<sub>y</sub> governed the leakage current, breakdown, and reliability. Usually SiO<sub>x</sub>N<sub>y</sub> is produced by thermal oxide annealing in NH<sub>3</sub>, NO, or N<sub>2</sub>O gas. Nitridation of SiO<sub>2</sub> in NH<sub>3</sub> results in the creation of a high density of electron traps in SiO<sub>x</sub>N<sub>y</sub>. To reduce the trap density, re-oxidation of SiO<sub>x</sub>N<sub>y</sub> usually follows after nitridation. Reoxidation results in the decrease of the electrons traps density. However, at the top interface SiO<sub>x</sub>N<sub>y</sub>/SiO<sub>2</sub> there is observed a high density of hole traps.<sup>7</sup> The nature of these traps is still unclear.

The aim of this paper is to investigate the physical structure of the Si<sub>3</sub>N<sub>4</sub>/thermal SiO<sub>2</sub> interface so as to understand the nature of traps at the interface and in silicon oxynitride. Two experimental techniques are employed for this purpose: electron energy loss spectroscopy (EELS) and ellipsometric measurements with chemical etching. Some preliminary results have been published.<sup>8</sup> This work describes a more complete and systematic investigation of excess silicon at the Si<sub>3</sub>N<sub>4</sub>/thermal SiO<sub>2</sub> interface.

### Sample Preparation and Measurement

The silicon-oxide-nitride-thermal oxide (SONO) structure was fabricated on a p-type silicon with orientation <100> or <111> and resistivity of about 10 Ω cm. A thin thermal oxide of 18 or 60 Å was first grown with dry oxidation and then a low pressure chemical vapor deposition (LPCVD) Si<sub>3</sub>N<sub>4</sub> was deposited on thermal oxide at 800°C using a mixture of SiCl<sub>4</sub> and NH<sub>3</sub>. The thickness of Si<sub>3</sub>N<sub>4</sub> was

150 Å for electron energy loss spectroscopy (EELS) to minimize charging effects, about 400 Å for ellipsometric measurements and 2200 Å for infrared absorption measurements. Thermal oxide on Si<sub>3</sub>N<sub>4</sub> was either native or produced by wet oxidation. Native oxide formed quickly when removing the sample from the hot LPCVD reactor to the atmosphere, whereas the wet oxidation was made at 900°C for 52 min. The ellipsometric measurements were performed using step-by-step etching of SONO structures in NH<sub>4</sub>F:HF = 7:1 solution at room temperature.

EELS measurements were conducted with Riber model LAS-3000 Auger electron spectrometer. The electron-beam with energy in the range of 100 to 3000 eV and 90° incident angle was used. The reflected electrons were measured at 42° with a cylinder mirror analyzer (see Fig. 1).

### Electron Energy Loss Spectroscopy

In the free electron approximation, the bulk plasmon energy ( $\hbar\omega_p$ ) is governed by the density of valence electrons ( $N_v$ ) and is given by

$$(\hbar\omega_p)^2 = 4\pi\hbar^2 e^2 N_v / m^* \quad [1]$$

where  $e$  and  $m^*$  are the charge and effective mass of electron, respectively. The density of valence electrons in Si<sub>3</sub>N<sub>4</sub> is governed by

$$N_v = N_A \rho \frac{n_{\text{Si}} + \frac{4}{3}n_{\text{N}}}{A_{\text{Si}} + \frac{4}{3}A_{\text{N}}} \quad [2]$$

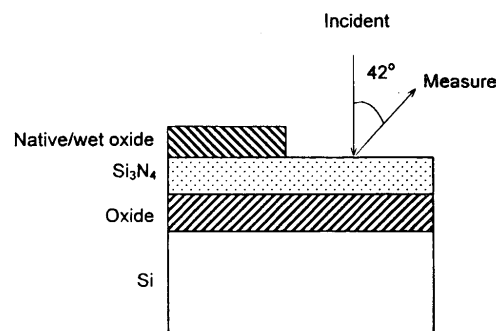


Figure 1. Illustration of sample structure and parameters for EELS measurements.

<sup>a</sup> Visiting Scholar at City University, Hong Kong.

<sup>b</sup> E-mail: vladimir@ee.cuhk.edu.hk or vladimir@isp.nsc.ru

where  $\rho$  is the  $\text{Si}_3\text{N}_4$  atomic density,  $N_A$  is the Avogadro number,  $A_{\text{Si}}$  and  $A_{\text{N}}$  are the atomic weights of silicon and nitrogen, respectively;  $n_{\text{Si}}$  and  $n_{\text{N}}$  are the numbers of valence electrons per silicon and per nitrogen atom taking part in the plasmon oscillation, respectively.

Since the density of valence electrons in  $\text{Si}_3\text{N}_4$ ,  $\text{SiO}_2$ , and Si are different, the bulk plasmon energies are also different in these materials. The electron mean free path (EMFP) in the solid state depends on the energy of the electrons. The higher the electron energy, the larger the EMFP. For instance at the excitation energy of 1486.6 eV, the Si 2p electrons with a binding energy of about 100 eV will have a kinetic energy of about 1380 eV and their EMFP at this kinetic energy is 21.1 Å in Si and 29.6 Å in  $\text{SiO}_2$ .<sup>9</sup> At excitation energy of 130 eV, the same Si 2p electrons will have a kinetic energy of about 30 eV and the mean free path is about 4 Å in Si and 7 Å in  $\text{SiO}_2$  only.<sup>10</sup> Hence bulk plasmon can be studied with high energy EELS and plasmon in thin surface layer can be investigated with low excitation energy.

Figure 2 shows the XPS loss spectra of  $\text{Si}_3\text{N}_4$ ,  $\text{SiO}_2$  and Si. The bulk plasmon energies ( $\hbar\omega_B$ ) for  $\text{Si}_3\text{N}_4$ ,  $\text{SiO}_2$ , and Si are 24.0 eV (from N 1s level), 23.0 eV (from O 1s), and 17.0 eV (from Si 2p), respectively. The accuracy of this measurement is about 1 eV. A more accurate (to about 0.3 eV) value of bulk plasmon energy had also been obtained by using high-energy (3000 eV) EELS measurements, and the results are depicted in Fig. 3. As shown in Fig. 3, the values of plasmon energies are the same as those obtained by XPS measurements. In addition, multiple plasmon excitations (three plasmons in Si and two plasmons in both  $\text{SiO}_2$  and  $\text{Si}_3\text{N}_4$ ) were observed which are indicated by arrows in Fig. 3. No surface plasmon with energy of  $\hbar\omega_B/\sqrt{2}$  was found. The 24.0 eV plasmon for  $\text{Si}_3\text{N}_4$  corresponds to  $n_{\text{Si}} = 4$  and  $n_{\text{N}} = 5$  at the  $\text{Si}_3\text{N}_4$  density  $\rho = 3.0 \text{ g/cm}^3$ .<sup>11</sup>

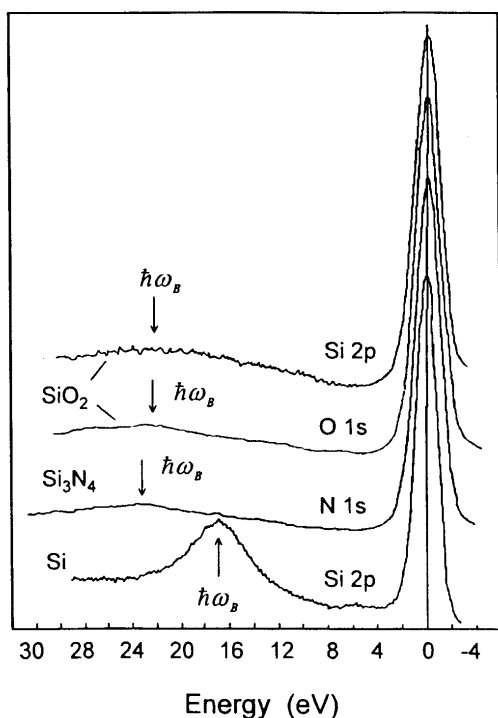


Figure 2. XPS electron energy loss spectra of  $\text{SiO}_2$ ,  $\text{Si}_3\text{N}_4$ , and Si.

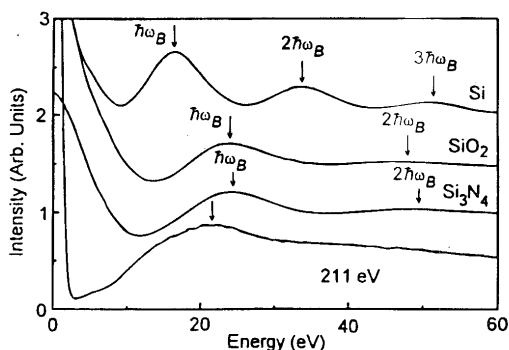


Figure 3. EELS spectra of bulk Si,  $\text{SiO}_2$  and  $\text{Si}_3\text{N}_4$  at electron-beam energy of 3000 eV (upper three curves) and EELS spectra with 211 eV beam energy for  $\text{Si}_3\text{N}_4$ /wet  $\text{SiO}_2$  interface after the top oxide was etched away (bottom curve).

Value  $n_{\text{N}} = 5$  is a result of the plasmon oscillation of (a) Si 3s, 3p, N 2p bonding; (b) N  $2p_{\pi}$  nonbonding nitrogen electrons of top valence band; and (c) two N 2s electrons of lower valence band.<sup>12</sup> This result is different from the conclusions drawn by Guraya et al.<sup>13</sup> who reported  $n_{\text{N}} = 3$  which corresponds to the plasmon oscillation from three p nitrogen electrons of the top valence band of  $\text{Si}_3\text{N}_4$ . To study the  $\text{Si}_3\text{N}_4$ /wet oxide interface, the top wet oxide is removed first and then a low energy (211 eV) electron-beam was used to probe the surface plasmon. As shown in Fig. 3, a wide plasmon peak with energy about 21-22 eV for  $\text{Si}_3\text{N}_4$ /wet  $\text{SiO}_2$  interface is observed.

Similar experiments were also conducted for the  $\text{Si}_3\text{N}_4$ /native  $\text{SiO}_2$  interface. The native oxide on  $\text{Si}_3\text{N}_4$  was etched away by using  $\text{HF}:\text{H}_2\text{O} = 1:30$  solution. The etching rate of  $\text{SiO}_2$  in this solution is about 1 Å/s [estimated by using X-ray photoelectron spectroscopy (XPS) measurement]. After the oxide layer was removed, EELS measurements with different electron-beam energy were conducted on the  $\text{Si}_3\text{N}_4$  surface. The decrease of electron-beam energy for EELS measurement gives rise to a low energy shift and a widened plasmon peak. As shown in Fig. 4, a plasmon peak at an energy of about 20 eV and with a large width was found at the electron-beam energy of 100 eV at the  $\text{Si}_3\text{N}_4$ /native  $\text{SiO}_2$  interface.

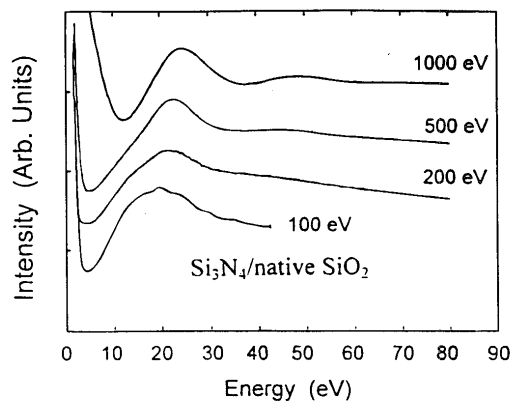


Figure 4. EELS of  $\text{Si}_3\text{N}_4$ /native  $\text{SiO}_2$  interface at different electron-beam energies after removal of top  $\text{SiO}_2$ .

Figure 5 shows the second derivative of EELS measurement for  $\text{Si}_3\text{N}_4$  after the surface native and wet  $\text{SiO}_2$  were removed. The high energy peaks with an energy of 20.3 and 21.1 eV can be seen clearly in the  $\text{Si}_3\text{N}_4$  films which were previously covered by native and wet oxide, respectively. These peaks are attributed to the plasmon oscillation in the transition layer at the  $\text{Si}_3\text{N}_4/\text{SiO}_2$  interface. The low energy peaks are probably due to defect excitations or interband transitions.

It is necessary to note that the second derivatives EELS are very sensitive to etching time and measurement conditions (electron beam energy and current). Plasmon losses at  $\text{Si}_3\text{N}_4/\text{native}$  or  $\text{Si}_3\text{N}_4/\text{wet SiO}_2$  interface with energy in the range 20–22 eV is lower than that of bulk  $\text{Si}_3\text{N}_4$  and bulk  $\text{SiO}_2$ . Hezel and Lieske<sup>14</sup> found that the plasmon at  $\text{Si}_3\text{N}_4/\text{native oxide}$  interface is 19.6 eV. Lifshiz et al.<sup>15</sup> also reported that the plasmon at  $\text{Si}_3\text{N}_4$  with native oxide decreases from 24 to 20 eV when the electron-beam energy changes from 2500 to 100 eV. Unfortunately, no explanation for the observation of low plasmon energy was proposed in these papers.

The decrease of the plasmon energy and the increase of the width of the peak by decreasing the electron beam energy can be explained as follows. A reduction in the electron energy results in the decrease of the EMFP and then reduces the plasmon energy relating to the plasmon losses in the transition layer at the  $\text{Si}_3\text{N}_4/\text{SiO}_2$  interface. First-order approximation can be made by assuming the low energy plasmon peak at 100 eV in Fig. 3 is composed by two peaks corresponding to  $\text{Si}_3\text{N}_4$  and Si. The EMFP in  $\text{SiO}_2$  measured at energy of 70 eV is about 6.6 Å,<sup>16</sup> and the effective width of the "silicon" interfacial layer, roughly equal to EMFP, is in the range of 6–8 Å which is consistent with the value proposed earlier by Lifshiz et al.<sup>15</sup>

It was found that the nonstoichiometric silicon nitride (with excess silicon) has a plasmon energy in the range of 17 to 24 eV.<sup>13,17</sup> Quali-

tatively the decrease of plasmon energy with the increase of excess silicon concentration can be explained with the following equation

$$N_v = \rho \frac{n_{\text{Si}} + x n_{\text{N}}}{A_{\text{Si}} + x A_{\text{N}}} L_A \quad [3]$$

where  $N_v$  is the density of valence electrons in  $\text{SiN}_x$ ,  $\rho$  is the  $\text{SiN}_x$  atomic density,  $A_{\text{Si}}$  and  $A_{\text{N}}$  are atomic weights,  $L_A$  is Avogadro number,  $n_{\text{Si}}$  and  $n_{\text{N}}$  are the numbers of valence electrons taking part in the  $\text{SiN}_x$  plasmon oscillation. The atomic density of  $\text{SiN}_x$  decreases from 3.0 g/cm<sup>3</sup> (for  $\text{Si}_3\text{N}_4$ ) to 2.33 g/cm<sup>3</sup> (for Si).

Similarly in the Si-enriched silicon oxide ( $\text{SiO}_{x/2}$ ), the plasmon energy changes from 22 eV (stoichiometric silicon oxide) to 17 eV (silicon).<sup>18</sup> The decrease of plasmon energy in  $\text{SiN}_x$  and  $\text{SiO}_x$  is attributed to the increase of the Si–Si bond concentration. The decrease of plasmon energy in the transition layer at the  $\text{Si}_3\text{N}_4/\text{SiO}_2$  interface can also be explained by the presence of Si–Si bonds at this interface.

It is more reasonable to expect that in general the transition layer at  $\text{Si}_3\text{N}_4/\text{SiO}_2$  interface consists of silicon-enriched silicon oxynitride (Si-rich  $\text{SiO}_x\text{N}_y$ ). Silicon oxynitride ( $\text{SiO}_x\text{N}_y$ ) may consist only of Si–O and Si–N bonds when it is grown at excess oxygen and nitrogen environment.<sup>19</sup> The  $\text{SiO}_x\text{N}_y$  film without Si–Si bonds consists of five sorts of tetrahedrons, i.e.,  $\text{SiO}_4$ ,  $\text{Si}_3\text{O}_7$ ,  $\text{Si}_2\text{O}_5$ ,  $\text{Si}_3\text{N}_4$ , and  $\text{Si}_2\text{N}_2\text{O}_2$ ,<sup>20–22</sup> and its plasmon energy between 22.0 eV ( $\text{SiO}_2$ ) and 24.0 eV ( $\text{Si}_3\text{N}_4$ ). However, our experiment shows that the plasmon energy at the  $\text{Si}_3\text{N}_4/\text{SiO}_2$  interface is in the range 20–22 eV. The discrepancy can be readily resolved by considering the excess silicon. The Si-rich  $\text{SiO}_x\text{N}_y$  consists of Si–O, Si–N, and Si–Si bonds.

#### Ellipsometric Measurements

Multiple angle ellipsometric measurements were carried out using a laser beam with a wavelength of 632.8 nm. Our parameter extraction software for the ellipsometer can restore four parameters simultaneously.<sup>23</sup> The measurement process is as follows. Top-down layer-by-layer etching and measurements were first performed until the Si substrate was reached. Then bottom-up parameter calculation process began, i.e., the lowest layer parameters,  $n_1$ ,  $d_1$ , (oxide on silicon) was calculated first and in the following steps four parameters ( $n_1$ ,  $d_1$  and  $n_2$ ,  $d_2$ ) were calculated simultaneously. During the measurements, we assumed that the layers being measured are transparent and homogeneous and the interlayer interface is abrupt. The etching time for each step was kept as small as possible to have a better resolution.

Before wet oxidation, the two-layer model was used in the calculation and the properties of the lower layer found in previous step was not considered. After wet oxidation, parameters  $n_i$  (where  $i = 3, 4, 5$ ) of the upper layers were determined with the single-layer model where the results found at previous steps were also taken into account. With wet oxidation, significant changes of the optical parameters (refractive index and thickness) are found in all regions (oxide on silicon, silicon nitride, and oxide on nitride regions) when compared to the previous ones.

The parameters  $n$  and  $d$  of thermal oxide on silicon were independently verified many times for structures with native oxide and with wet oxidation. Unfortunately, accuracy of the refractive index is poor if the film thickness is less than 100 Å. The accuracy is within  $\pm 2\%$  from median value of  $n_1$  and  $\pm 5\%$  from median value of  $d_1$ . The variations give rise from (i) measurement errors, (ii) precision of ellipsometer, and mainly (iii) exactness of the same positioning at each step.

It is well known that Si,  $\text{SiO}_2$ , and  $\text{Si}_3\text{N}_4$  have distinct values of refractive indexes; their typical values are 3.42, 1.46, and 1.96, respectively. Enriching  $\text{SiN}_x$  or  $\text{SiO}_x$  with excess silicon results in the increase of their refractive indexes.<sup>22</sup> Figure 6 shows the refractive index as a function of the depth of the ONO structure before (with native oxide) and after wet oxidation. The refractive index  $n = 2.1$  of the interfacial layer of  $\text{Si}_3\text{N}_4/\text{wet oxide}$  system is significantly larger than 1.96 which is typical for the bulk of amorphous  $\text{Si}_3\text{N}_4$ . Although we did not detect any refractive index larger than

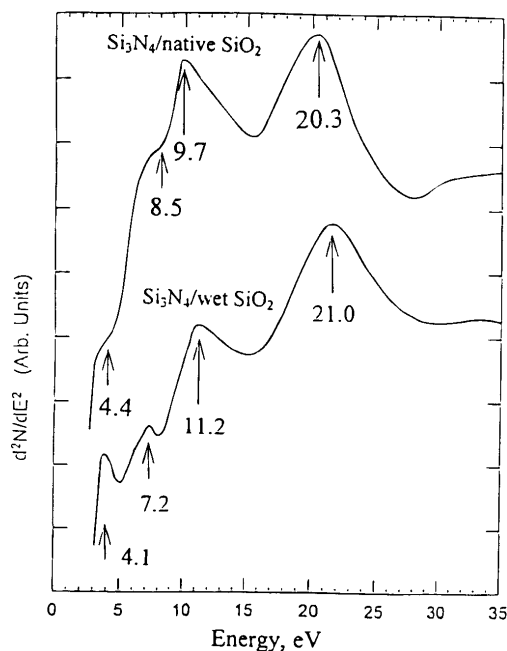


Figure 5. Second derivative of EELS of  $\text{Si}_3\text{N}_4/\text{native SiO}_2$  and  $\text{Si}_3\text{N}_4/\text{wet SiO}_2$  interfaces measured at an electron-beam energy of 200 eV after the top oxide layer was removed.

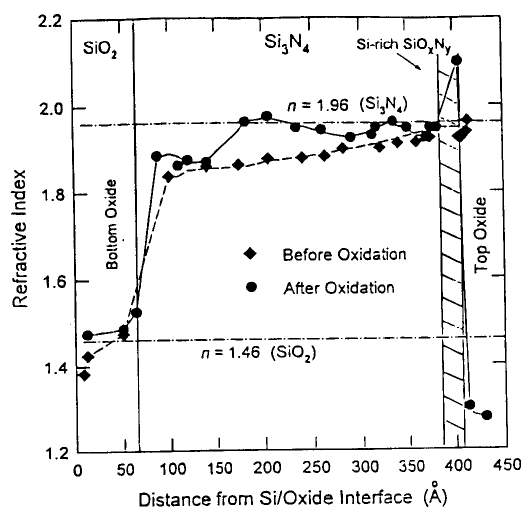


Figure 6. Refractive index of Si/SiO<sub>2</sub>/Si<sub>3</sub>N<sub>4</sub>/SiO<sub>2</sub> with native oxide (before oxidation) and wet oxide after oxidation) at different depths.

1.96 before wet oxidization, we cannot ascertain that there is no excess silicon at the interface as the step resolution for etching and ellipsometric measurements is still quite large.

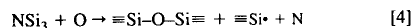
To sum up, we have found from both EELS and ellipsometric measurements that excess silicon (Si-Si bonds) exist at the Si<sub>3</sub>N<sub>4</sub>/thermal SiO<sub>2</sub> interface. The interfacial layer may be in the form of SiN<sub>x</sub>, SiO<sub>x</sub>, or Si-rich SiO<sub>x</sub>N<sub>y</sub>. Wet oxidation of Si<sub>3</sub>N<sub>4</sub> results in the change of optical properties in Si<sub>3</sub>N<sub>4</sub>, bottom SiO<sub>2</sub>, and top SiO<sub>2</sub> films (see Fig. 6 and 7). In addition, oxidation also results in the change of etching rate of Si<sub>3</sub>N<sub>4</sub>, bottom oxide, and top oxide (see Fig. 8). In the following section possible mechanisms for these changes are discussed in detail.

#### Change of Dielectric Refractive Index during ONO Structure Synthesis

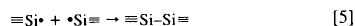
In this section, possible chemical reactions are discussed and the change of optical properties of dielectric layers in ONO structures at different fabrication steps are explained.

**Creation of Si-Si bonds at Si<sub>3</sub>N<sub>4</sub>/thermal SiO<sub>2</sub> interface.**—The excess Si-Si bonds were observed in the present work at both Si<sub>3</sub>N<sub>4</sub>/native SiO<sub>2</sub> and Si<sub>3</sub>N<sub>4</sub>/wet SiO<sub>2</sub> interfaces. In following sections the possible reactions for both structures are discussed.

**Native oxidation.**—Generally the Si-Si bond creation during the Si<sub>3</sub>N<sub>4</sub> oxidation in dry atmosphere can be understood based on the Mott rule. According to this rule, each Si atom in SiO<sub>2</sub>, Si<sub>2</sub>N<sub>4</sub>, or SiO<sub>x</sub>N<sub>y</sub> is coordinated by four O and/or N atoms, each O atom in SiO<sub>2</sub>, SiO<sub>x</sub>N<sub>y</sub> is coordinated by two Si atoms and each N atom in Si<sub>3</sub>N<sub>4</sub> or SiO<sub>x</sub>N<sub>y</sub> is coordinated by three Si atoms.<sup>22</sup> Substitution of N atom by O atom during Si<sub>3</sub>N<sub>4</sub> dry oxidation accompanies the creation of a three-coordinated silicon atom with an unpaired electron ≡Si•



Two such silicon atoms with unpaired electrons result in the creation of an Si-Si bond, namely



The overall reaction can be written as

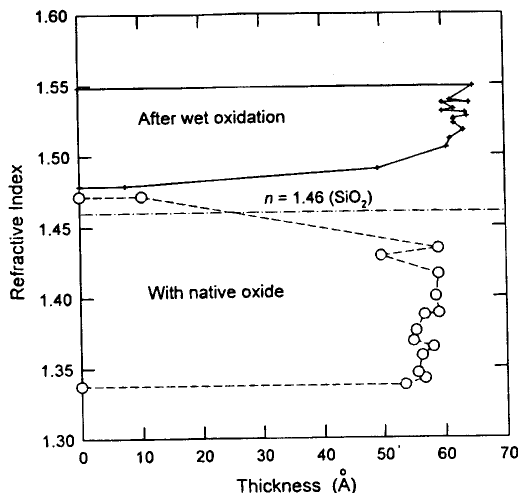
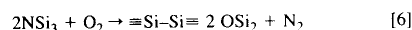
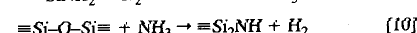
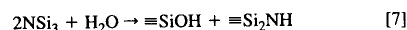


Figure 7. Comparison of restored thickness and refractive index of the bottom thermal oxide in Si/SiO<sub>2</sub>/Si<sub>3</sub>N<sub>4</sub>/SiO<sub>2</sub> structure before (with native oxide) and after wet oxidation.

**Wet oxidation.**—The chemical reactions relating to the Si-Si bond creation during wet oxidation are more complicated. Possible reactions are given below<sup>24-26</sup>



Reactions 6-13 describe, on the atomic scale, the creation of Si-Si bonds at the Si<sub>3</sub>N<sub>4</sub>/SiO<sub>2</sub> interface during the silicon nitride oxidation in terms of chemical bond rearrangements. The Si-Si bonds at Si<sub>3</sub>N<sub>4</sub>/SiO<sub>2</sub> interface are part of the SiSi<sub>2</sub>O<sub>2</sub>N<sub>2</sub> tetrahedrons in

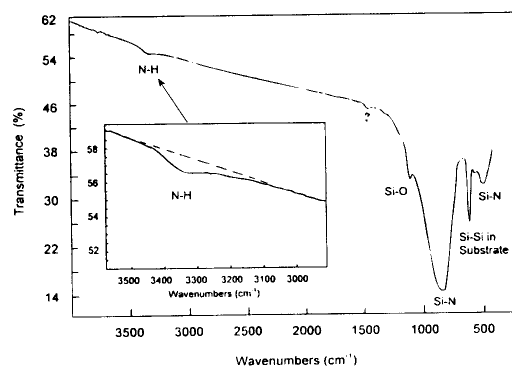
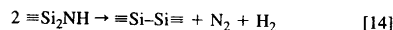


Figure 8. Infrared absorption of Si/SiO<sub>2</sub> (60 Å)/Si<sub>3</sub>N<sub>4</sub> (2200 Å)/SiO<sub>2</sub> structure before (solid) and after (dashed) wet oxidation.

which  $\alpha$ ,  $\beta$ ,  $\delta = 0, 1, 2, 3, 4$ , and  $\alpha + \beta + \delta = 4$ . These tetrahedrons build the Si-rich  $\text{SiO}_x\text{N}_y$ .

**Increase of  $\text{Si}_3\text{N}_4$  refractive index after oxidation.**—As shown in Fig. 6, the refractive index of bulk  $\text{Si}_3\text{N}_4$  increases after wet oxidation. This effect can be explained with the out-diffusion of hydrogen from  $\text{Si}_3\text{N}_4$  during the wet oxidation and the creation of Si–Si bonds. For  $\text{Si}_3\text{N}_4$  with a high concentration of NH bonds, the release of hydrogen and nitrogen from the nitride was observed experimentally after the sample was annealed in vacuum.<sup>27</sup> This result could be due to the following reaction



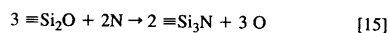
According to Eq. 14, hydrogen is released from silicon nitride. This process will accompany the creation of the Si–Si bond. The Si–Si bond creation during the annealing of  $\text{Si}_3\text{N}_4$  has been confirmed experimentally with the shift of the fundamental absorption edge to the lower energy side in infrared measurements.<sup>22,27</sup> As measured with the infrared absorption spectroscopy the silicon nitride (after synthesis with native oxide) has an absorption band in infrared region and centered at  $3330 \text{ cm}^{-1}$  which is attributed to the absorption of  $\text{Si}_2\text{NH}$  bond (see Fig. 8). The concentration of NH bonds in this sample is about  $2 \times 10^{21} \text{ cm}^{-3}$ . Wet oxidation results in the decrease of NH bonds and reduces the infrared absorption. The proposed explanation also agrees with the decrease of etching rate of silicon nitride after oxidation. It is well known that the decrease of hydrogen bond density in silicon nitride would also result in the decrease of the etching rate.<sup>20</sup>

**Optical properties of bottom oxide.**—Figure 7 indicates the refractive index of the bottom  $\text{SiO}_2$  on Si before and after wet oxidation. The data depicted in Fig. 7 clearly shows the changes of  $\text{SiO}_2$  properties after wet oxidation. Both the thickness and the refractive index of the bottom  $\text{SiO}_2$  increase after the  $\text{Si}_3\text{N}_4$  film was oxidized. The average refractive index before wet oxidation is less than 1.46 (a typical value for thermal oxide on silicon). It is greater than 1.46 after wet oxidation, however.

The refractive index of dry thermal oxide with a thickness of about 50 Å before  $\text{Si}_3\text{N}_4$  deposition was 1.46. Deposition of  $\text{Si}_3\text{N}_4$  results in the decrease of oxide refractive index (Fig. 7) and the increase of etching rate (Fig. 8). These two phenomena can be explained by the oxide hydrogenation (reaction 12). The hydrogen atoms, which escape from  $\text{Si}_3\text{N}_4$  bottom layers (reaction 14) during  $\text{Si}_3\text{N}_4$  deposition further react with  $\text{SiO}_2$  and produce Si–OH and Si–H bonds. Hydrogen-containing oxide often has a smaller refractive index. It is well known that low temperature (CVD)  $\text{SiO}_x\text{H}$  film which contains a large density of hydrogen (and appeared as SiOH and SiH bonds) has refractive indexes smaller than the thermal  $\text{SiO}_2$ .<sup>28</sup> Similarly, the refractive index of PECVD  $\text{SiN}_x\text{H}$  film with a large density of N–H and Si–H bonds has a refractive index smaller than that of a nitride with a small density of hydrogen.<sup>29</sup> In addition, it is well known that the increase of hydrogen contamination in  $\text{SiO}_x\text{H}$  and  $\text{SiN}_x\text{H}$  film results in the decrease of etching rate. These results agree with the experimental results depicted in Fig. 9.

**Optical properties of bottom oxide after  $\text{Si}_3\text{N}_4$  oxidation.**—The increase of bottom oxide refractive index after  $\text{Si}_3\text{N}_4$  deposition can be explained with the following mechanisms.

**Nitridation of bottom oxide at  $\text{Si}_3\text{N}_4$  oxidation.**—Nitrogen escaped from the bulk  $\text{Si}_3\text{N}_4$  during wet oxidation can diffuse into the bottom oxide and results in the following reaction



The replacement of O atoms in the bottom  $\text{SiO}_2$  by N atoms results in the formation of oxynitride. It is well known that the refractive index will be increased by increasing the nitrogen concentration in  $\text{SiO}_x\text{N}_y$ .<sup>20</sup> The oxygen, which is released after the replacement reaction 15, diffuses into  $\text{SiO}_2$  and results in the further oxidation of silicon substrate. This effect explains the increase of the bottom  $\text{SiO}_2$  thickness after the silicon nitride was oxidized.

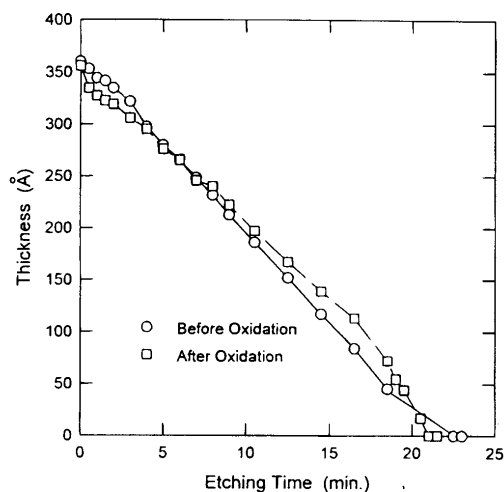
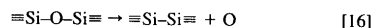


Figure 9. Plot of the thickness of  $\text{Si/SiO}_2/\text{Si}_3\text{N}_4/\text{SiO}_2$  structure vs. the etching time for the structure before and after wet oxidation.

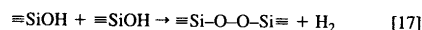
**Reduction of bottom oxide after  $\text{Si}_3\text{N}_4$  oxidation.**—Another possible mechanism for the increase of the bottom oxide refractive index after  $\text{Si}_3\text{N}_4$  oxidation is the enriching of  $\text{SiO}_2$  by excess silicon due to creation of oxygen vacancies as proposed Devine,<sup>30</sup> the reaction is



Oxygen diffusion from the bottom  $\text{SiO}_2$  into Si results in the creation of  $\text{SiO}_{x-2}$  and oxidation of silicon substrate.

It is possible that both mechanisms 15 and 16 take part in the increase of the refractive index and further growth of the bottom oxide. However, present results cannot differentiate between reactions 15 and 16.

**Optical properties of oxide produced by  $\text{Si}_3\text{N}_4$  oxidation.**—The refractive index of the top oxide in the ONO structure is smaller than that of the dry thermal oxide on silicon (see Fig. 6). The low value of the refractive index in the top oxide may be due to the hydrogenation effect of the top oxide, i.e., creation of Si–OH and Si–H bonds according to reaction 12. Excess oxygen contamination in the top oxide may also give rise to the low value of the refractive index. Excess oxygen may exist in the form of the peroxide bridge Si–O–O–Si. The peroxide bridge forms on the top oxide at high temperatures according to the following reaction<sup>31</sup>



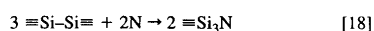
## Discussion

The direct evidence of the existence of excess silicon at  $\text{Si}_3\text{N}_4/\text{native SiO}_2$  interface in ONO structures was obtained by qualitative analyses using XPS measurement with high-resolution chemical etching.

The evidence of excess silicon at the  $\text{Si}_3\text{N}_4/\text{wet}$  and  $\text{Si}_3\text{N}_4/\text{native SiO}_2$  interfaces in this work are the low values of plasmon energy and large width of plasmon peak at the interface. Our newly proposed model can also interpret the low value plasmon energy obtained by others.<sup>14,15</sup> The plasmon with energy 19.6 eV at  $\text{Si}_3\text{N}_4/\text{native oxide}$  interface, obtained by Lieske and Hezel,<sup>14</sup> can be attributed to the existence of Si-rich  $\text{SiO}_x\text{N}_y$  at the interface. For  $\text{Si}_3\text{N}_4$  with the native oxide, the plasmon energy decreases from 24 to 20 eV by lowering the electron-beam energy from 2500 to 100 eV. This was observed previously by Lifshiz et al.<sup>15</sup> and can be explained by the existence of Si-rich  $\text{SiO}_x\text{N}_y$  at the  $\text{Si}_3\text{N}_4/\text{native SiO}_2$

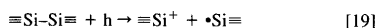
interface. However, Lieske and Hezel<sup>32</sup> obtained a low "bulk plasmon" energy (18.6 eV) in Si<sub>3</sub>N<sub>4</sub>. This result is inconsistent with our data and the value (24.0 eV) obtained by Lifshiz et al. The discrepancy can be explained as follow. In Lieske and Hezel's experiments,<sup>32</sup> the "bulk plasmon" energy was determined by bombarding the Si<sub>3</sub>N<sub>4</sub> and with Ar<sup>+</sup> ions. It was shown that the Ar<sup>+</sup> bombardment of Si<sub>3</sub>N<sub>4</sub> would reduce the nitrogen concentration on the surface, forming Si-rich Si<sub>3</sub>N<sub>4</sub>.<sup>33</sup> The decrease of SiN<sub>x<2</sub> density results in the decrease of plasmon energy.<sup>13,17</sup>

On the other hand, the ellipsometric measurements of SONO structures do not provide direct evidence of the existent of excess silicon at Si<sub>3</sub>N<sub>4</sub>/native SiO<sub>2</sub> interface. Similar results were observed by others.<sup>34,35</sup> However, excess silicon does exist at the Si<sub>3</sub>N<sub>4</sub>/wet SiO<sub>2</sub> interface. With spectroscopic ellipsometric measurements, Theeten et al.<sup>36</sup> found that there exists an amorphous silicon layer of about 12 Å between the nitride/native oxide layers in the SONO structures. Silicon accumulates after the sample was annealed in NH<sub>3</sub> at 900°C. This observation was explained with the interaction between excess Si-Si bonds and nitrogen according to the following reaction



Reaction 18 also explains the removal of Si-Si bonds after the SiO<sub>2</sub> was nitrated.<sup>38</sup> Reaction 18 also explains the accumulation of excess silicon at the Si<sub>3</sub>N<sub>4</sub>/native SiO<sub>2</sub> interface in SONO structures. Although excess silicon was not observed by using ellipsometric measurements,<sup>34,35</sup> AES profile interface had shown the existence of a notable amount of excess silicon at Si<sub>3</sub>N<sub>4</sub>/wet SiO<sub>2</sub> interface.<sup>36</sup> Hence, a more systematic ellipsometric investigation of excess silicon in SONO structures is needed in order to clarify this discrepancy.

It is well known that there are some  $\equiv \text{Si}_3\text{N}$  species on the top surface of SiO<sub>2</sub>N<sub>x</sub> after nitridation of SiO<sub>2</sub>,<sup>38</sup> and it was shown that, at the top surface of reoxidized SiO<sub>2</sub>N<sub>x</sub>, the existence of a high density of E' centers was observed.<sup>7</sup> E' centers are created after a hole was captured on a Si-Si bond according to reaction



It is natural to propose that the Si-Si bonds at the SiO<sub>x</sub>N<sub>y</sub>/thermal SiO<sub>2</sub> interface are created by replacing nitrogen atoms with oxygen atoms according to reaction 6. The numerical simulation of Si-Si electronic structure shows that these defects in silicon oxide and silicon nitride may act as electron and hole traps.<sup>39-42</sup> These results together can be used to explain the abnormally large electron and hole capturing at the Si<sub>3</sub>N<sub>4</sub>/thermal SiO<sub>2</sub> interface.<sup>3-6</sup> However, the results obtained in the present work show that the oxidation mechanism of Si<sub>3</sub>N<sub>4</sub> is more complicated than that based only on transformation of Si-N bonds in Si<sub>3</sub>N<sub>4</sub> into Si-O bonds. In fact, some unusual kinetics of Si<sub>3</sub>N<sub>4</sub> oxidation are observed.<sup>43,44</sup> Hence we suggest that the creation of Si-Si bond at Si<sub>3</sub>N<sub>4</sub> oxidation should be taken into account.

### Conclusions

Excess silicon at Si<sub>3</sub>N<sub>4</sub>/thermal native and wet oxide interfaces has been qualitatively studied by using EELS and ellipsometric measurements. The main results are as follows.

1. With EELS measurements we found that the plasmon energy of the transition layer at the Si<sub>3</sub>N<sub>4</sub>/thermal oxide interface is lower than that of Si<sub>3</sub>N<sub>4</sub> and SiO<sub>2</sub>. Plasmon peaks at the interface have larger widths than those of Si<sub>3</sub>N<sub>4</sub> and SiO<sub>2</sub>.

2. Ellipsometric measurements show a large value (2.1) of the refractive index in the transition layer. It is the evidence of the existence of excess Si-Si bonds at Si<sub>3</sub>N<sub>4</sub>/wet SiO<sub>2</sub> interface.

3. Wet oxidation of Si<sub>3</sub>N<sub>4</sub> results in the increase of the refractive index of the bottom oxide and nitride in ONO structures. Changes of refractive index of the dielectric layers in ONO structure after the wet oxidation of Si<sub>3</sub>N<sub>4</sub> are qualitatively explained in terms of chemical reaction in solid state.

4. The above observations are interpreted in terms of the Si-rich SiO<sub>x</sub>N<sub>y</sub> layer at the Si<sub>3</sub>N<sub>4</sub>/thermal SiO<sub>2</sub> interface. The estimated width of this layer is in the range of 6-8 Å.

5. The Si-Si bond creation during Si<sub>3</sub>N<sub>4</sub> oxidation is explained with the Mott rule. Replacement of the threefold coordinated N atom by twofold coordinated O atom result in the creation of Si-Si defects.

### References

- P. C. Fazan, A. Ditali, C. H. Dennison, H. E. Rhodes, H. C. Chan, and Y. C. Liu, *J. Electrochem. Soc.*, **138**, 2052 (1991).
- S. Minami and Y. Kamigaki, *IEEE Trans. Electron. Devices*, **ED-40**, 2011 (1993).
- E. Suzuki, Y. Hayashi, K. Ishi, and T. Tsuchiya, *Appl. Phys. Lett.*, **42**, 608 (1983).
- A. P. Aganin, V. M. Maslovskii, and A. P. Nagin, *Microelectron. (Sov.)*, **17**, 348 (1988).
- Z. A. Weinberg, K. J. Stein, T. N. Nguen, and J. Y. Sun, *Appl. Phys. Lett.*, **57**, 1248 (1990).
- H. S. Momose, T. Morimoto, Y. Ozawa, K. Yamabe, and H. Iwai, *IEEE Trans. Electron. Devices*, **ED-42**, 704 (1995).
- J. T. Yount, P. M. Lenahan, and G. J. Dunn, *IEEE Trans. Nucl. Sci.*, **NS-39**, 2211 (1992).
- V. A. Gritsenko, I. P. Petrenko, S. N. Svitashva, and H. Wong, *Appl. Phys. Lett.*, **72**, 462 (1998).
- Z. H. Lu, J. P. McCaffrey, B. Brar, G. D. Willk, R. M. Wallace, L. C. Feldman, and S. P. Tay, *Appl. Phys. Lett.*, **71**, 2784 (1997).
- F. Rochet, Ch. Poncey, G. Dutour, H. Roulet, C. Guillot, and F. Sirotti, *J. Non-Cryst. Solid*, **216**, 148 (1997).
- V. P. Bolotin, I. A. Brytov, V. A. Gritsenko, B. Z. Olshanezki, V. P. Popov, Yu. N. Romashenko, V. G. Serapin, and S. A. Tiis, *Sov. Phys. Dokl.*, **310**, 114 (1990) in English.
- V. A. Gritsenko, Yu. N. Morokov, and Yu. N. Novikov, *Solid State Phys.*, **39**, 1191 (1997).
- M. M. Guraya, H. Ascolani, G. Zampieri, J. I. Cisneros, J. H. Diasda Silva, and M. P. Cantao, *Phys. Ref. B*, **49**, 5677 (1990).
- R. Hezel and N. Lieske, *Inst. Phys. Conf. Series*, No. 50, Chap. 3, p. 206 (1980).
- V. G. Lifshiz, V. G. Kotlar, and A. A. Saranin, *Surface (Sov.)*, **12**, 76 (1984).
- J. Himpfel, F. R. McFeely, A. Tabel-Ibragimi, J. A. Yarmoff, and G. Hollinger, *Phys. Rev. B*, **38**, 6084 (1988).
- R. Karcher, L. Ley, and R. L. Johnson, *Phys. Rev. B*, **30**, 1896 (1984).
- F. G. Bell and L. Ley, *Phys. Rev. B*, **37**, 8383 (1988).
- I. A. Brytov, V. A. Gritsenko, and Yu. N. Romashenko, *Sov. Phys. JETP*, **89**, 321 (1985) in English.
- V. A. Gritsenko, in *Silicon Nitride in Electronics*, pp. 138-187, Elsevier, New York (1988).
- V. A. Gritsenko, N. D. Dikovskaja, and K. P. Mogilnikov, *Thin Solid Films*, **51**, 353 (1978).
- V. A. Gritsenko, *Structure and Electronic Properties of Amorphous Dielectrics in Silicon MIS Structures*, p. 280, Science, Novosibirsk, Russia (1993).
- Yu. E. Voskoboinikov, E. V. Lantukhova, and S. N. Svitashva, *Optoelectron. Instrum., Data Process.*, **4**, 99 (1996).
- F. H. P. M. Habraken, E. H. C. Ullersama, W. M. Arnoldbik, and A. E. T. Kuiper, in *Proceedings of the NATO Advanced Research Workshop: Fundamental Aspects of Ultrathin Dielectrics in Si-Based Devices toward an Atomic Scale Understanding*, pp. 411-424, Kluwer Academic Pub., Boston, MA (1997).
- J. E. Shelby, *J. Appl. Phys.*, **52**, 2589 (1980).
- K. M. Davis, A. Agarwal, M. Tomozawa, and K. Hirao, *J. Non-Cryst. Solid*, **203**, 27 (1996).
- L. V. Chramova, T. P. Chusova, V. A. Gritsenko, G. N. Feofanov, and T. P. Smirnova, *Nonorgan. Mater. (Sov.)*, **23**, 73 (1987).
- I. I. Belousov, V. A. Gritsenko, and V. M. Efimov, *Surface (Rus.)*, **10**, 62 (1992).
- Z. Yin and F. W. Smith, *Phys. Rev. B*, **42**, 3666 (1990).
- R. Devine, *J. Phys. III*, **6**, 1569 (1996).
- K. Awazu and H. Kawazoe, *J. Non-Cryst. Solid*, **179**, 214 (1994).
- R. Hezel and N. Lieske, *Thin Solid Films*, **61**, 217 (1979).
- R. S. Bhattarya and P. H. Holloway, *Appl. Phys. Lett.*, **38**, 545 (1981).
- S. Trolier-McKinstry, H. Hu, and A. H. Carim, *J. Electrochem. Soc.*, **141**, 2483 (1994).
- T. S. Chao, C. L. Lee, and T. F. Lei, *J. Appl. Phys.*, **73**, 1732 (1993).
- J. B. Theeten, D. E. Aspnes, F. Simondet, M. Erman, and P. C. Murau, *J. Appl. Phys.*, **52**, 6788 (1981).
- V. A. Gritsenko, in *Proceedings of NATO Advanced Research Workshop: Fundamental Aspects of Ultrathin Dielectrics in Si-Based Devices toward an Atomic Scale Understanding*, pp. 335-342, Kluwer Academic Pub., Boston, MA (1997).
- E. C. Carr and R. A. Buhman, *Appl. Phys. Lett.*, **63**, 55 (1993).
- V. A. Gritsenko, Yu. N. Morokov, Yu. N. Novikov, H. Wong, and Y. C. Chen, in *Mater. Res. Soc. Symp. Proc.*, **446**, (Amorphous and Crystalline Insulating Thin Films), pp. 169-173, Kluwer Academic, Pub., Boston, MA (1997).
- V. O. Sokolov and V. B. Sulimov, *Phys. Status Solidi B*, **135**, 369 (1986).
- J. K. Rudra and W. B. Fowler, *Phys. Rev. B*, **35**, 8223 (1987).
- W. L. Warren and P. M. Lenahan, *Phys. Rev. B*, **42**, 1773 (1990).
- K. L. Luthra, *J. Electrochem. Soc.*, **138**, 3001 (1991).
- T. Enomoto, R. Ando, H. Morita, and H. Nakayama, *Jpn. J. Appl. Phys.*, **17**, 1049 (1978).